Modeling analysis of the seasonal characteristics of haze formation in Beijing

X. Han[1], M. Zhang[1,*] J. Gao[2], S. Wang[2], and F. Chai[2]

[1] State Key Laboratory of Atmospheric Boundary Layer Physics and Atmospheric Chemistry, Institute of Atmospheric Physics, Chinese Academy of Sciences, HuaYanBeiLi 40#, Chaoyang District, Beijing 100029, China

[2] Chinese Research Academy of Environmental Sciences, Beijing 100012, China

Correspondence to: M. Zhang (mgzhang@mail.iap.ac.cn)

Abstract. The air quality modeling system RAMS-CMAQ coupled with an aerosol optical property scheme was applied to simulate the meteorological field, major aerosol components (sulfate, nitrate, ammonium, black carbon, organic carbon, dust, and sea salt), and surface visibility over the North China Plain (NCP) in 2011. The modeled results in February and July 2011 were selected and analyzed to obtain an in-depth understanding of the haze formation mechanism in Beijing in different seasons. The evaluations suggested that the modeling system provided reliable simulation results of meteorological factors (temperature, relative humidity, wind field, and precipitation), visibility, mass concentrations of gaseous pollutants (NO_2 and O_3), and major aerosol components in $PM_{2.5}$ by compared with various observation data at several measurement stations over NCP. The simulation results showed that the visibility below 10 km covered most regions of NCP and dropped below 5 km over Beijing and Tianjin megacities, the whole area of Hebei province, and northwest part of Shandong province during the pollution episodes in February and July. The heavy mass concentration of $PM_{2.5}$ ranged from 120 μg m^{-3} to 300 μg m^{-3} were concentrated in the same areas as well. The haze formation mechanism in Beijing in winter is obviously different from that in summer. The mass concentration of $PM_{2.5}$ in winter is relatively higher and the components are complicated. The ratios of inorganic salts and carbonaceous aerosols are generally balanced. Therefore, the high mass concentration of $PM_{2.5}$ and diverse aerosol components should be the major reasons of the serious haze occurrence in winter. While the mass concentration of $PM_{2.5}$ in summer is relatively lower than that in winter, but the ratio of hygroscopic inorganic salts, including sulfate, nitrate and ammonium, increased and their mass concentrations were even higher than

those in winter. With obviously higher relative humidity, it can still form serious haze with equal level to winter even the mass concentration of $PM_{2.5}$ is lower than that in winter. The water uptake of hygroscopic aerosols plays a key role in it. Moreover, the analysis shows that the influence of $PM_{2.5}$ mass burden on visibility is very weak when its value located in a high level (larger than 100 μg m^{-3}). Only when the mass burden of $PM_{2.5}$ decreases to a certain threshold interval can the visibility increase rapidly. This indicates that when emission reduction measures are taken to control haze occurrence, the mass burden of $PM_{2.5}$ must be cut down below this certain threshold interval. A sensitivity test was conducted to estimate the $PM_{2.5}$ mass concentration threshold of haze occurrence in Beijing. The relative humidity and contribution ratio of accumulation particles to extinction are two important impact factors which could obviously change the threshold when the aerosol components do not have dramatic variation. Furthermore, since the change of the contribution ratio of accumulation particles generally occurs in clean period, the relative humidity should be the only impact factor which needs to be considered. The relationship between threshold of haze occurrence and relative humidity in winter and summer in Beijing was fitted by the exponential function, and these fitting curves could be a new theoretical basis for the further understanding and control of the haze formation in Beijing.

1. Introduction

The emissions of air pollutants have recently increased significantly because of the economic growth, rapid population expansion, and urbanization in the North China Plain (NCP). Beijing, which is the capital of P. R. China, has a population of over 20 million and is the political, economic, and cultural center of China. This megacity is located at the northern tip of NCP and surrounded by high mountains in its northern and western boundaries. Beijing has suffered from air quality deterioration in the past decade because of strong local emissions (Sun et al., 2006) and long-range transport from the surrounding urban areas (Zhang et al., 2012) located in the east and south of NCP; such areas include Tianjin, Shijiazhuang, and a number of cities where the economic development is most active in Hebei Province. The air pollution in Beijing is easily aggravated by its special geographic position when stable weather appears or the south wind dominates. Although the SO_2 emission in Beijing in the last five years has been decreased by various measures prescribed by the current legislation on emission controls (Lu et al., 2010; Zhang et al., 2006), the mass burden of particulate pollutants remains at a high level (Hao et al., 2013; Zhang et al., 2013), causing serious environmental issues and associated health effects.

Atmospheric haze is caused by the visibility deterioration (lower than 10 km, Wu et al., 2007) through light extinction by aerosol particles. As a result of the high level of aerosol loadings, widespread haze cloud caused by serious air pollution occurred more frequently over this region in the past decade (Ma et al., 2010; Tao et al., 2012; Wang et al., 2013; Zhao, et al., 2011). A number of studies have investigated the long-term variation features of haze days in Beijing and NCP. Quan et al. (2011) collected monitoring data and summarized the haze day occurrence trend over NCP for the past 56 years. These researchers also analyzed the effect of high aerosol loadings on haze formations by conducting a field measurement and found the important role of the hygroscopic growth of aerosols during the haze period. Yu et al. (2010) analyzed the aerosol optical properties during haze days in the past seven years and compared the features of single-scattering albedo and asymmetry factor during haze days with those during dust days in Beijing. This study also found that fine-mode particles were dominant in aerosol size distribution during haze days.

Numerous studies have used multiple methods to investigate the chemical and physical properties of aerosols during haze occurrences in Beijing in different seasons. Li et al. (2013) identified the aerosol size distribution and chemical composition from ground-based remote sensing measurements during haze days in winter. Li et al. (2010) detected the aerosol components by using transmission electron microscopy with energy-dispersive X-ray spectrometry during a haze episode in summer and determined the influence of carbonaceous aerosols. Liu et al. (2013) and Zhao et al. (2013) conducted intensive field experiments to identify the aerosol components of fine particles and discussed the constituent features of $PM_{2.5}$ during the haze periods in autumn and winter, respectively. Wang et al. (2006) compared the characteristics of aerosol components during dust, haze, and clean days. These previous works have provided abundant information on the physical and chemical properties of aerosols during haze days. However, the complex mechanism of haze formation over Beijing and its surrounding regions requires further study. Various influencing factors, including meteorological field, key aerosol components, and microphysical properties, should be comprehensively considered in investigating the relationship between aerosols and surface visibility. Moreover, the seasonal similarities and differences of the haze formation mechanism in Beijing remain unclear because most of these studies were generally focused on the pollution periods in the same season.

In the present study, an air quality modeling system called Regional Atmospheric Modeling System–Community Multi-scale Air Quality (RAMS–CMAQ) coupled with aerosol optical property

scheme is applied to simulate the meteorological field, the mass burden of major aerosol components (sulfate, nitrate, ammonium, black carbon (BC), organic carbon (OC), dust, and sea salt), and the surface visibility over NCP in 2011. The simulation results in February and July 2011 are selected and analyzed. This study aims to discuss the contributions of various influencing factors to visibility deterioration and to compare the differences of the haze formation mechanisms during winter and summer.

2. Methodology

The air quality modeling system RAMS–CMAQ was applied to concurrently simulate the atmospheric and land processes that affect the transport, transformation, and deposition of aerosols and their precursors. The major component of this modeling system is CMAQ (version 4.7), which was developed by the US Environmental Protection Agency for assessing the effect of multiple pollutants, including tropospheric ozone and other oxidants, aerosols, and acid deposition (Byun and Schere, 2006; Eder and Yu, 2006; Eder et al., 2009; Mathur et al., 2008). The gas-phase chemistry mechanism was updated to the expanded version CB05 (Sarwar et al., 2008). The thermodynamic equilibrium between inorganic aerosol species and gas-phase concentrations was treated by ISORROPIA (Nenes et al., 1999). Regional Particulate Model (Binkowski and Shankar, 1995) was used to describe the processes of aerosol dynamics in CMAQ; such processes include new particle production, coagulation, and condensation (Bhave et al., 2004; Yu et al., 2013). The formation of secondary organic aerosol (SOA) was mainly treated by the CB05 mechanism, which was extended to allow for production of SOA from anthropogenic and biogenic precursors. In the CB05, the SOA formation is modeled by forming semi-volatile products in volatile organic compounds (VOCs) reactions. The semi-volatile products are partitioned between the gas and aerosol phase according to the ambient conditions, such as temperature, relative humidity, vapor pressure, existing aerosol particles. The aerosol particles in the modeling system were divided into three modes, namely, Aitken, accumulation, and coarse modes (dust and sea salt). All modes were assumed to follow the log normal distribution. The aerosol components, the geometric standard deviation, and the geometric mean radius of each mode are listed in Table 1. The numerical prediction model RAMS was coupled with CMAQ in the offline method to provide CMAQ with a meteorological field. A general description of RAMS and its capabilities have been provided by Cotton et al. (2003). RAMS can describe the boundary layer and the underlying surface effect, which is important for capturing air pollutants and haze occurrence. The background meteorological fields and sea surface temperature were obtained from

the European Center for Medium-Range Weather Forecasts reanalysis datasets (1° × 1° spatial resolution) and were based on weekly mean values and observed monthly snow cover information, respectively.

The anthropogenic emissions of precursors and primary aerosols (NO_x, SO_2, VOCs, BC, OC, $PM_{2.5}$, and PM_{10}) were obtained from the monthly-based emission inventory in China for 2010. This emission inventory has a spatial resolution of 0.25° × 0.25° and includes four categories, namely, power, industry, residential, and transport (Lu et al., 2011). The nitrogen oxides and ammonia from soil were adopted from the Global Emissions Inventory Activity 1° × 1° monthly global inventory (Benkovitz et al., 1996). The monthly mean inventory of Global Fire Emissions Database Version 2 (Randerson et al., 2007) was used to provide the biomass burning emissions from forest wildfires, savanna burning, and slash-and-burn agriculture. The online mechanisms introduced by Han et al. (2004) and Gong (2003) for capturing dust and sea salt emissions, respectively, were included in the modeling system.

A scheme of aerosol optical properties was added to the modeling system to estimate the aerosol extinction coefficient. This scheme contains a parameterization (Ghan and Zaveri, 2007) that efficiently simplifies Mie theory calculation and maintains sufficient accuracy. Briefly speaking, the lognormal distribution in each mode can be expressed as:

$$\frac{dN}{d\ln D}=\frac{N}{(2\pi)^{1/2}\ln\sigma_g}\exp\left(-\frac{(\ln D-\ln D_p)^2}{2\ln^2\sigma_g}\right) \quad (1)$$

where N is the number concentration of aerosol particles, σ_g is the geometric standard deviation, D is the particle diameter, and D_p is the geometric mean diameter. If refractive index and σ_g are given and the N is set as a normalized value, the aerosol optical properties can be calculated by the Mie theory under several D_p. It has been proved that 40 D_p ranging from maximum to minimum particle diameters of each mode are sufficient for errors less than 10% under most conditions. Then, the specific optical properties under these 40 D_p could be fitted by the Chebyshev polynomials with just five fitting coefficients. Subsequently, the fitting coefficients table can be constructed with all possible values of refractive index and σ_g. The scheme also applies Kohler theory (Pruppacher and Klett, 1997) and Maxwell–Garnett mixing rule (Chuang et al., 2002) to describe the effects of water uptake and internal mixture, respectively. The detailed description of this scheme can be found in Han et al. (2011). The visibility can be obtained by using the following equation:

$$VIS = 3.912/\beta \quad (1)$$

where VIS is the horizontal visibility, and β is the aerosol extinction coefficient (Seinfeld and Pandis,

1998). This modeling system simulated the mass concentration and optical properties of key aerosols in previous studies on aerosol effects on the climate and environment in China (Han et al., 2013; Han et al., 2011; Zhang et al., 2005, 2006, 2007).

For the simulation over NCP, a coarse domain that covers most of East Asia with a horizontal grid distance of 64 km and a total area of 6654 km × 5440 km with a two-way nested inner domain was established (Han et al., 2011). The inner domain (Fig. 1) has 94 × 90 grid cells and a 16 km resolution on a rotated polar stereographic map projection centered at (116 °E, 40 °N). This domain includes all major regions in NCP, namely, Beijing, Tianjin megacities and Hebei, Shandong, Shanxi provinces. Fifteen vertical levels, nearly half of which were concentrated in the lowest 2 km, were used to improve the simulation of the atmospheric boundary layer. The positions of the measurement stations applied for model evaluation are marked on Fig. 1. The district areas of four major cities: Beijing, Tianjin, Shijiazhuang, and Jinan were also shown in Fig. 1.

3. Model evaluation

In this section, the model simulations are compared with the observations. The meteorological driver is an important factor in aerosol and visibility simulation. Wind vector, temperature, and relative humidity are inherently related to aerosol transport, scavenging, and water uptake effect. Thus, the monitoring data from the surface stations of the Chinese National Meteorological Center (CNMC; (http://cdc.cma.gov.cn/home.do) were collected to evaluate the performance of the meteorological field simulation. CNMC has 726 measurement stations that are evenly distributed throughout mainland China and has been providing long-term surface observations of several meteorological variables since 1 January 1951 (Feng et al., 2004).

The comparative results of the daily average temperature, relative humidity, wind speed, and maximum wind direction at eight stations in February and July are shown in Figs. 2 to 5, respectively. The modeled temperature, relative humidity, and wind speed were in good agreement with the observations at nearly all stations. A persistent underestimation of wind speed by the models was found at the Wutaishan and Taishan sites. The modeled wind speed presented in Fig. 4 was obtained by converting the output values of the first layer (90 m to 200 m) to near-surface wind (~10 m) according to Monin–Obukhov similarity theory (Ding et al., 2001). These two sites are located on the mountainside at elevations of 2208 and 1533 m, respectively, thus, the underestimation may be attributed to the different

elevations between the simulation and the observation. As shown in Fig. 5, the modeled wind directions did not coincide well with the observed data. A direct comparison is difficult to achieve because of the difference in time resolutions between the site measurements (10 min, average) and the model output (1 h). Nevertheless, the variation trends of the modeled and observed wind directions are similar at most sites, as shown in Fig. 5. The monthly modeled precipitation over NCP was compared to the observations of surface monitoring data from 87 CNMC sites in Fig. 6. It can be seen that the modeling system generally performed well on capturing the distribution patterns and seasonal variation features of precipitation in Beijing, Tianjin megacities and Inner Mongolia, Hebei, Shandong provinces. However, the modeled results kindly underestimated the precipitation in North Beijing and north part of Hebei province in July, which could cause the error of wet deposition estimation. The comparison of modeled and observed precipitation in Beijing will be discussed in detail below.

The modeled hourly NO_2, O_3, $PM_{2.5}$, and visibility in February and July were also compared with the observed data provided by the Chinese Research Academy of Environmental Sciences (CRAES); CRAES observes the real-time mass burden of air pollutants in Beijing (Gao et al., 2012). The comparative results are shown in Figs. 7 and 9. The statistical parameters, including means, standard deviations, and correlation coefficients between observation and simulation are listed in Table 2. These metrics can be used to evaluation of model performance (Yu et al., 2006). The model efficiently captured the daily variation of the pollutant gases and the high mass burden of $PM_{2.5}$ in these two months as shown in Fig. 7. Table 2 shows that most of the correlation coefficients are higher than 0.6, and the means and standard deviations of simulations are also similar to those of observations. However, the correlation coefficients of $PM_{2.5}$ and NO_2 are lower than 0.5 in July. From Fig.7 and the means and standard deviations in Table 2, it can be found that the model generally overestimated $PM_{2.5}$ in the middle of July, and the fluctuation range of modeled NO_2 was larger than that of the observation results. The comparison of modeled and observed daily precipitation in Beijing is given in Fig. 8 (the observation data was collected from CNMC). It can be seen that the modeled precipitation in July was obviously lower than that of observation in the middle of July. This may result in weaker wet deposition which can cause overestimation of aerosol burden in Beijing. For the simulated NO_2, the lager diurnal variation may be just caused by the uncertainties from related gas-phase chemical scheme in ISORROPIA. The modeled visibility also agrees well with the observations, particularly for visibility lower than 10 km, suggesting that the model can provide reasonable simulation during haze occurrence. The means and standard deviations of modeled

visibility are quite similar to those of observations. Meanwhile, continuous haze can be found in the modeled and observed results in the middle of July, as shown in Fig. 9. This phenomenon indicates that although the model overestimated the mass burden of $PM_{2.5}$, the visibility simulation during this period remains reliable.

The modeled daily average mass concentrations of major aerosol components were compared with the observed data from the CRAES measurements, as shown in Fig. 10. The observed data lacked information for the first half of February and a number of days in July because of instrument failure. Although the magnitudes of the mass concentrations between the simulation and the observation do not exactly agree with each other, the modeled results could broadly reproduce the peaks of the observed data from February 20 to February 23 and from July 20 to July 23; the modeled results could also follow the seasonal variation features. For instance, the modeled and observed carbonaceous aerosols were both high in February and low in July. The model demonstrated obvious systematic underestimation of organic carbon in these two months, as shown in Fig. 10. Numerous studies have reported that such phenomenon is a common issue in regional chemistry and transport models (Heald et al., 2005; Koch et al., 2007). The simulation error is primarily due to the uncertainties in the estimation of VOCs and primary organic aerosol emissions and the formation mechanism of secondary organic aerosol (Kroll et al., 2006; Henze and Seinfeld, 2006; Yu et al., 2007). However, this discrepancy should not significantly affect the accuracy of the visibility simulation. Therefore, these evaluations suggest that the modeling system can reasonably simulate the meteorological field, the mass burdens of major aerosol components, and the surface visibility in February and July 2011.

4. Results and discussions

4.1 Distribution features of aerosol concentration and visibility

As shown in Figs. 7 to 10, two typical heavy air pollution episodes occurred over NCP from February 20 to February 23 and from July 20 to July 23. These two periods were selected to investigate the distribution features of pollutants and visibility over NCP during occurrences of heavy pollution in different seasons. Fig. 11 presents the horizontal distributions of daily average mass concentration of $PM_{2.5}$ and surface wind field over NCP from February 20 to February 23 and from July 20 to July 23. The heavy mass burden of $PM_{2.5}$ (over 120 $\mu g\ m^{-3}$) was mainly concentrated in Beijing and Tianjin megacities, the whole area of Hebei province and northwest part of Shandong province. The mass concentration of

$PM_{2.5}$ in February, which exceeded 200 μg m^{-3} in Beijing, Tianjin, Shijiazhuang, and Jinan, was obviously higher than that in July. The high mass burden of $PM_{2.5}$ appeared in the same regions as those in February broadly ranged from 75 μg m^{-3} to 200 μg m^{-3} in July, and was rarely over 200 μg m^{-3} over the entire NCP. The high mass burden of $PM_{2.5}$ in Beijing generally appeared when NCP was dominated by the south wind field, which could have brought pollutants from the polluted regions in the south. The heavy $PM_{2.5}$ mass burden was also possibly transported to Northeast China and Bohai Sea by the strong south wind from February 22 to February 23 and on July 23, respectively, thereby increasing the mass concentration of $PM_{2.5}$ by 45 μg m^{-3} to 125 μg m^{-3} in these two regions, as shown in Fig. 11.

Fig. 11 also presents the horizontal distributions of daily average visibility and surface relative humidity over NCP. The data shows that haze cloud could spread throughout NCP during each pollution episode. The visibility in most parts of Hebei and Shandong was generally less than 8 km, which could decrease to 3 km to 5 km in the four urban areas in February and July. The distribution patterns of visibility broadly followed those of the $PM_{2.5}$ mass burden, and deteriorated visibility mainly appeared in the regions where the heavy $PM_{2.5}$ mass burden is concentrated. The visibility generally decreased to 3 km to 5 km when the mass concentration of $PM_{2.5}$ exceeded 200 μg m^{-3} in February. However, similar values of visibility also appeared in July when the mass concentration of $PM_{2.5}$ was merely in the range of 120 μg m^{-3} to 200 μg m^{-3}. Such phenomenon was demonstrated on July 23 when the visibility over the entire Bohai Sea generally ranged from 3 km to 5 km and the mass concentration of $PM_{2.5}$ was maintained between 120 and 200 μg m^{-3}. These differences may be due to the strong extinction of soluble particles caused by the high relative humidity (exceeding 70%) in July, as shown in Fig. 11. This feature is discussed in detail below.

4.2 Meteorological factors, major aerosol components and their contributions to extinction in Beijing

Figs. 12(a) to 12(h) present the time series of regional average surface wind speed, and relative humidity, visibility, as well as the mass concentrations of $PM_{2.5}$, sulfate, nitrate, ammonium, BC, and OC in Beijing in February and July 2011. The averages of these variables during the haze days in February and July are shown in Table 3. The mass burden of $PM_{2.5}$ is the most important influencing factor of visibility change because it is generally inversely correlated with the variation of visibility. The mass concentrations of three kinds of inorganic salt, namely, nitrate, sulfate, and ammonium, suggest that they were the three major aerosol components of $PM_{2.5}$ in Beijing, as shown in Figs. 12(e) to 12(f). Nitrate was the main particulate pollutant during winter because the mass burden of nitrate was obviously higher than

those of the other components in February. Although the diurnal variation of nitrate concentration was significant in July, the daily maximum nitrate concentration was still larger than that of sulfate concentration during nighttime. These findings suggest that the emission from the transportation sector is currently the major source of secondary particles in Beijing. The mass burden of carbonaceous aerosols was high in February and low in July. In addition to the diffusion conditions, the strong emissions of coal and biomass burning are the main reasons for the high values of carbonaceous aerosols during winter.

As shown in Table 3, July had a greater number of haze days than February, and the average visibility during haze days in July was lower than that in February. These features indicate that air pollution was more serious in July than in February. However, the average mass concentration of $PM_{2.5}$ in July during haze days was obviously lower than that in February. In addition, Table 3 shows that the relatively low value of $PM_{2.5}$ mass concentration in July was primarily due to the small quantities of carbonaceous aerosol burden. Meanwhile, the total mass burden of nitrate, sulfate, and ammonium was higher in July than in February. Therefore, the deteriorated visibility is caused by the simultaneous occurrence of high mass burden of soluble particles and high relative humidity in July. The difference in the haze formation mechanism during winter and summer should be associated with the different constructions of $PM_{2.5}$ components and the ambient relative humidity.

Fig. 12(g) to 12(h) present the time series of the regional average contribution ratios of sulfate, nitrate, ammonium, BC, OC, and other components (dust, sea salt, and unspecified anthropogenic mass) to the total surface extinction in Beijing in February and July. The monthly mean of these contribution ratios are shown in Table 4. The contribution ratios were calculated by subtracting the extinction coefficient with and without each aerosol component when estimated the aerosol optical properties by using the scheme introduced in section 2. Nitrate, sulfate, and ammonium, which are inorganic salts, significantly contributed to the surface extinction in Beijing, which was ~70% in February and over 80% in July. Carbonaceous aerosol provided nearly 20% and 5% contribution in February and July, respectively, whereas other aerosol components provided ~10% contribution. These ratios generally followed the magnitude of their mass concentrations. Except for the diurnal variation of nitrate in July, the contribution ratios of each aerosol component did not significantly change when the mass concentration of $PM_{2.5}$ exceeded ~50 $\mu g\ m^{-3}$. By contrast, when the mass concentration of $PM_{2.5}$ decreased to less than 50 $\mu g\ m^{-3}$, the contribution ratios of carbonaceous aerosol and other components obviously increased. A higher mass concentration of $PM_{2.5}$ corresponds to higher contribution ratios of

the three inorganic salts. This feature confirms that nitrate, sulfate, and ammonium are the major aerosol components that influence the haze formation in Beijing.

4.3 Haze occurrence threshold in Beijing

It can be seen from Fig. 12 that the mass concentration of $PM_{2.5}$ was closely inversely correlated with visibility. However, when the mass concentration of $PM_{2.5}$ located in different value intervals, the influence on the visibility was not consistent. Fig. 13 shows the time series of regional mean mass concentration of $PM_{2.5}$ and visibility in Beijing from 23 to 25 July. As is seen, the air qualities in these three days turned to good and the visibility continuously increased. The mass concentration of $PM_{2.5}$ decreased from 260 μg m^{-3} on 23 July to 20 μg m^{-3} on 25 July. For the convenience of distinguishing, the decreasing process is divided into A, B and C periods in the figure. Then, it can be found that in A period, the mass concentration of $PM_{2.5}$ changed from 260 μg m^{-3} to 120 μg m^{-3}, decreasing by about 140 μg m^{-3} while the visibility increased by less than 5km; in B period, the mass concentration of $PM_{2.5}$ changed from 120 μg m^{-3} to 50 μg m^{-3}, decreasing by about 70 μg m^{-3} and the visibility increased obviously, from 5km to about 20km; finally, in C period, the mass concentration of $PM_{2.5}$ changed from 35 μg m^{-3} to 20 μg m^{-3}, decreasing by only 15 μg m^{-3} and the visibility increased dramatically by 60km. The above analysis indicated that even though the emission reduction measures are taken to dramatically decrease the $PM_{2.5}$ mass burden, the improvement of visibility would still be weak if the mass concentration of $PM_{2.5}$ keeps in a high level. Only when the mass concentration of $PM_{2.5}$ is decreased to the certain value range can the visibility be improved greatly and it is easier for the visibility to be over 10km. Therefore, strictly speaking it is necessary to distinguish the atmospheric haze and the atmospheric pollution. The improvement of atmospheric quality (mass concentrations of pollutants decrease) does not mean the haze disappears. If the occurrence of haze is controlled by decreasing mass concentration of $PM_{2.5}$ in atmosphere, it is more reasonably to set a haze occurrence threshold interval (the values of mass concentration of $PM_{2.5}$ when the visibility reaches 10 km in different ambient conditions). Only by strictly keeping the mass concentration of $PM_{2.5}$ below this threshold can the visibility be effectively improved. Otherwise, even though the emission reduction measures are taken when heavy pollution event appears, the improvement of visibility would still be very weak if the mass concentration of $PM_{2.5}$ fails to fall into the values of haze occurrence threshold. Furthermore, the specific value of the threshold should be closely related to the pollutant characteristics, meteorological conditions and other factors.

A sensitivity test was conducted to evaluate the mass concentration threshold of $PM_{2.5}$ to cause haze

329 occurrence in Beijing. First, the mass ratio of each aerosol component to the total mass burden of all
330 aerosol particles was calculated from the results of the model simulation at every grid point. Then, the
331 sensitivity run was conducted by using several possible values of the total aerosol burden and following
332 the same ratio of each aerosol component at the same grid points to identify the mass concentration
333 threshold of $PM_{2.5}$ when the visibility decreased to 10 km under different relative humidity. The values of
334 relative humidity were chosen as follows: 70%, 75%, 80%, 85%, 88%, 89%, and 90%. Lower values of
335 relative humidity were disregarded because the water uptake of soluble particles is insignificant when the
336 relative humidity is less than 70%. Figs. 14(a) and 14(b) present the time series of the regional average
337 threshold of haze occurrence under different values of relative humidity from the sensitivity test in
338 February and July in Beijing. The threshold changed significantly with the variation in relative humidity,
339 and its declining trend increased with increasing relative humidity. The range of mass concentration
340 threshold reached 30 μg m^{-3} when the relative humidity changed from 70% to 90%. Conversely, the
341 threshold generally maintained a small value range (<5 μg m^{-3}) when the relative humidity was fixed.
342 This indicated that if the aerosol components do not have dramatic variation in Beijing, a relatively fixed
343 haze occurrence threshold could be determined.

344 However, the mass concentration threshold on July 29 could increase by approximately 10 μg m^{-3}
345 under the same relative humidity, as shown in Fig. 14(b). Further analysis showed that this phenomenon
346 might be related to the variation of aerosol in accumulation mode. Figs. 14(c) to 14(h) present the time
347 series of the regional average mass ratios and contribution ratios of the three particle modes to the total
348 aerosol burden and the total extinction, respectively. As is seen from Fig. 14(e) and 14(h), the extinction
349 contribution of accumulation mode particles was above 97% due to the high mass concentration ratio and
350 extinction efficiency. However, it can be found that the extinction contribution of accumulation mode
351 particles on 29 July obviously decreased by about 5%. Therefore, it can be deduced there should be a high
352 correlation between the haze occurrence threshold and extinction contribution of accumulation mode
353 particles. Furthermore, it can be seen from Fig. 14(j) that the visibility on 29 July rose from less than 5km
354 to more than 20km rapidly. Thus, it can be deduced that a weather process which was beneficial to the
355 pollutant scavenging eliminated the mass concentration of accumulation mode particles efficiently (the
356 new particles in the atmosphere could be eliminated immediately before coagulation or condensation) in
357 this period. Then, the mass concentration ratio and extinction contribution ratio of Aitken mode particles
358 could be increased about 10% and 5%, respectively. These should be the major reason for the decreasing

359 extinction contribution ratio of accumulation mode particles. The similar weather processes also occurred
360 on 2-3, 5-10, and 25 July. It can be found that during these periods the mass concentration of
361 accumulation mode particles decreased significantly. However, different from the condition on 29 July,
362 the mass concentration ratio and extinction contribution of Aitken mode particles did not change
363 obviously, but the mass concentration ratio of coarse mode particles increased dramatically in these three
364 processes. It is found that though the mass concentration of coarse mode particles accounted for 10%-20%
365 of the total aerosol, its extinction contribution was only below 1% in most periods. Therefore, except
366 some special cases (e. g., dust event), the influence of coarse mode particles on extinction should be
367 obviously weaker than other modes. This was also the main reason for no significant variation of
368 extinction contribution ratio of accumulation mode particles in these three processes.

369 Generally speaking, besides relative humidity, haze occurrence threshold is also sensitive to the
370 extinction contribution ratio of accumulation mode particles. Seen from the above analysis, the mass
371 concentration ratio of accumulation mode particles generally remained at high level and the fluctuation
372 range was small during the heavy pollution episode in Beijing, which can ensure the variation range of
373 haze occurrence threshold was less than 5 μg m^{-3} when the relative humidity was fixed. The increase of
374 haze occurrence threshold due to the variation of extinction contribution of accumulation mode particles
375 only appeared when the mass burden of Aitken mode particles increased in clean period. The reason for
376 this phenomenon should be that the extinction efficiency of Aitken mode particles is far smaller than that
377 of accumulation mode particles. Therefore, more Aitken mode particles are needed to form the haze.
378 However, the smaller particles generally exist during the clean period as shown by the simulation results,
379 which means the haze does not appear. Thus, the influence of extinction contribution of accumulation
380 mode particles on haze occurrence threshold can be neglected in Beijing in most cases. The relative
381 humidity should be the only impact factor which needs to be considered.

382 The monthly means of the threshold of haze occurrence are shown in Table 5. It can be seen from
383 Table 5 that when the relative humidity changed from 70% to 90%, the threshold interval increased from
384 52 μg m^{-3} to 83 μg m^{-3}. In a certain relative humidity, the average monthly thresholds were similar in
385 February and July. Here, the relationship between haze occurrence threshold and relative humidity was
386 fitted by the exponential function, and below is the formula:

387 $$RH = a + b \times \exp(c \times M) \quad (2)$$

388 where, RH represents relative humidity; M represents the $PM_{2.5}$ mass concentration threshold; a, b and c

represent fitting parameters, and their values are listed in Table 6. The fitting curve is shown in Fig. 15. From Table 6 it can be seen that the values of R^2 are all higher than 0.9, which indicates that their relationship can be described by exponential function well. Therefore, the fitting curves given in Fig. 15 can be used to capture the haze occurrence threshold in Beijing. In a certain relative humidity, when $PM_{2.5}$ mass concentration increases beyond the corresponding values on the curve, the haze should be easy to appear. Furthermore, the analysis in this study also indicated that the haze occurrence can be efficiently controlled by strictly restricting the $PM_{2.5}$ mass concentration near or below the fitting curve. Otherwise, the greatly decrease of $PM_{2.5}$ mass burden would not obviously reduce the possibility of haze occurrence.

5. Conclusions

In this study, the air quality modeling system RAMS-CMAQ coupled with an aerosol optical property scheme was used to simulate the meteorological field, the mass concentration of aerosols, and the surface visibility over NCP in 2011. The modeling system provided reliable simulation results. The distribution patterns and time series of related meteorological factors and aerosol characteristic in February and July 2011 were analyzed to elucidate the seasonal variation features of the haze formation mechanism in Beijing and its surrounding regions. In addition, a sensitivity test was conducted to investigate the $PM_{2.5}$ mass concentration threshold of haze occurrence in Beijing under distinct conditions. The results are summarized as follows:

(1) The simulation results showed that the high mass burden of $PM_{2.5}$ over NCP was mainly concentrated in Beijing and Tianjin megacities, the whole area of Hebei province and northwest part of Shandong province. The daily average mass concentration of $PM_{2.5}$ over these regions was generally over 120 μg m^{-3} during the pollution episodes in February and July. The worst air quality over NCP was found in Beijing because of the heavy daily average mass burden of $PM_{2.5}$, which exceeded 300 μg m^{-3} in February. The south wind that carries pollutants from the southern regions is an important source of the heavy aerosol loading in Beijing. In addition to the horizontal diffusion, the vertical convection also plays an important role in the pollutant scavenging in Beijing.

(2) The distribution patterns of visibility generally followed those of the $PM_{2.5}$ mass burden. The daily average visibility below 10 km covered most regions of NCP during the pollution episodes in February and July and was below 5 km over the urban areas. The daily average relative humidity rarely exceeded 90%, suggesting that the haze cloud could spread throughout NCP when the pollution episode

appears in both winter and summer.

(3) The simulation results showed that nitrate, sulfate, and ammonium were the three major aerosol components and the main causes of the visibility deterioration in Beijing. The mass burdens of these three inorganic salts were obviously higher than those of other aerosols, and their total contribution ratios to surface extinction reached 70% in February and 85% in July. Nitrate was also the first and second major contributor to surface extinction in February and July, respectively, implying that the emission from the transportation sector is currently the major source of secondary particles in Beijing. The carbonaceous aerosols accounted for 15% extinction in February and below 5% extinction in July. This feature indicates that the pollution status and emission sources were more complicated during winter in Beijing.

(4) The haze formation mechanism in Beijing in winter is obviously different from that in summer. Firstly, the mass concentration of $PM_{2.5}$ in winter was relatively higher and the components were complicated. The ratios of inorganic salts and carbonaceous aerosols were generally balanced. Therefore, the high mass concentration of $PM_{2.5}$ and diverse aerosol components should be the major reasons of the serious haze occurrence in winter. While the mass concentration of $PM_{2.5}$ in summer was relatively lower than that in winter, but the ratio of hygroscopic inorganic salts, including sulfate, nitrate and ammonium, increased and their mass concentrations were even higher than those in winter. With obviously higher relative humidity, it could still form serious haze with equal level to winter even the mass concentration of $PM_{2.5}$ is lower than that in winter. The water uptake of hygroscopic components played a key role in it. This indicated that it is important to apply emission reduction measures based on the specific pollution and meteorological characteristics in different seasons. In this way, the possibility of haze occurrence can be effectively decreased.

(5) From analysis, it can be found that even though the mass concentration of $PM_{2.5}$ is closely inversely correlated with visibility, the influence effect is diversity when the mass concentration of $PM_{2.5}$ locates in different intervals. When the mass concentration of $PM_{2.5}$ is relatively high (larger than 100 μg m^{-3}), the influence of its variation on visibility is very weak. Only when the mass concentration of $PM_{2.5}$ is cut down to a certain interval can its decrease make the visibility increase rapidly. Therefore, it is more reasonably to set a haze occurrence threshold interval (the values of mass concentration of $PM_{2.5}$ when the visibility reaches 10 km in different ambient conditions). If the mass concentration of $PM_{2.5}$ fails to fall into the values of haze occurrence threshold, the improvement of visibility would still be very weak when the emission reduction measures are taken.

(6) Through the sensitivity experiment, this study estimated the haze occurrence threshold interval in Beijing, and discussed related impact factors. Generally speaking, if the components of $PM_{2.5}$ do not have dramatic variation in Beijing, the haze occurrence threshold is just sensitive to the extinction contribution ratio of accumulation mode particles and relative humidity. In consideration of the variation of extinction contribution ratio of accumulation mode particles generally occurs in the clean period, the relative humidity should be the only impact factor which needs to be considered. Finally, the relationship between threshold of haze occurrence and relative humidity in winter and summer in Beijing was fitted by the exponential function, and these fitting curves could be a new theoretical basis for the further understanding and control of the haze formation in Beijing.

Reference

Benkovitz, C., Schultz, M., Pacyna, J., Tarrason, L., Dignon, J., Voldner, E., Spiro, P., Logan, J., and Graedel, T.: Global gridded inventories of anthropogenic emissions of sulfur and nitrogen, J. Geophys. Res., 101, 29239-29254, 1996.

Bhave, P. V., Roselle, S. J., Binkowski, F. S., Nolte, C. G., Yu, S. C., Gipson, G. L., and Schere, K. L.: CMAQ Aerosol Module Development: Recent Enhancements and Future Plans, Paper presented at 3rd Annual CMAS Models-3 Users' Conference, Commun. Model., and Anal. Syst. Cent., Chapel Hill, N.C., 18-20 October, 2004.

Binkowski, F. S. and Shankar, U.: The regional particulate model, 1, Model description and preliminary results, J. Geophys. Res., 100, 26191-26209, 1995.

Byun, D. and Schere, K.: Review of the governing equations, computation algorithms, and other components of the Models-3 Community Multiscale Air Quality (CMAQ) modeling system. Appl. Mech. Rev., 59, 51-77, 2006.

Chuang, C., Penner, J., Prospero, J., Grant, K., Rau, G., and Kawamoto, K.: Cloud susceptibility and the first aerosol indirect forcing: sensitivity to black carbon and aerosol concentrations, J. Geophys. Res.，107, doi: 10.1029/2000JD000215, 2002.

Cotton, W., Pielke, R., Walko, G., Liston, G., Tremback, C., Jiang, H., McAnelly, R., Harrington, J., Nicholls, M., Carrio, G., and McFadden, J.: RAMS 2001: current status and future directions, Meteorol. Atmos. Phys., 82, 5-29, 2003.

Ding, F., Pal Arya, S., and Lin, Y.: Large-eddy simulations of the atmospheric boundary layer using a new subgrid-scale model-II. Weakly and moderately stable cases, Environ. Fluid Mech., 1, 49-69, 2001.

Eder, B., Kang, D., Mathur, R., Pleim, J., Yu, S. C., Otte, T., and Pouliot., G.: A performance evaluation of the national air quality forecast capability for the summer of 2007, Atmos. Environ., 43, 2312-2320, 2009.

Eder, B. and Yu, S. C.: An evaluation of model performance of EPA models-3/CMAQ, Atmos. Environ., 40, 4811-4824, 2006.

Feng, S., Hu, Q., and Qian,W.: Quality control of daily meteorological data in China, 1951-2000: a new dataset. Int. J. Climatol., 24, 853-870, 2012.

Gao, J., Zhang, Y., Wang, S., Chi, F., and Chen, Y.: Study on the Characteristics and Formation of a Multi-Day Haze in October 2011 in Beijing, Res. Environ. Sci. (in Chinese), 25, 1201-1207, 2012.

Ghan, S., and Zaveri, R.: Parameterization of optical properties for hydrated internally mixed aerosol, J. Geophys. Res., 112, D10201, doi:10.1029/2006JD007927, 2007.

Gong, S. L.: A parameterization of sea-salt aerosol source function for sub- and super-micron particles, Global Biogeochem. Cy., 17, doi: 10.1029/2003GB002079, 2003.

Han, X., Zhang, M., Han, Z., Xin, J., and Liu, X.: Simulation of aerosol direct radiative forcing with RAMS-CMAQ in East Asia, Atmos. Environ., 45, 6576-6592, 2011.

Han, X., Zhang, M., Tao, J., Wang, L., Gao, J., Wang, S., Chai, F.: Modeling aerosol impacts on atmospheric visibility in Beijing with RAMS-CMAQ, Atmos. Environ., 72, 177-191, 2013.

Han, Z., Ueda, H., Matsuda, K., Zhang, R., Arao, K., Kanai, Y., and Hasome, H.: Model study on particle size segregation and deposition during Asian dust events in March 2002, J. Geophys. Res., 109, doi: 10.1029/2004JD004920, 2004.

Hao, J. and Wang, L.: Improving Urban Air Quality in China: Beijing Case Study, Air Waste Manage. Assoc., 62, 1298-1305, 2012.

Heald, C. L., Jacob, D. J., Park, R. J., Russell, L. M., Huebert, B. J., Seinfeld, J. H., Liao, H., and Weber, R. J.: A large organic aerosol source in the free troposphere missing from current models, Geophys. Res. Lett., 32, L18809, doi:10.1029/2005GL023831.

Henze, D. K. and Seinfeld, J.H.: Global secondary organic aerosol from isoprene oxidation, Geophys. Res. Lett, 33:L09812, doi:10.1029/2006GL025976, 2006.

Koch, D., Bond, T. C., Streets, D., Unger, N., van der Werf, G. R.: Global impact of aerosols from particular source regions and sectors, J. Geophys. Res., 112, D02205, doi:10.1029/2005JD007024, 2007.

Kroll, J. H., Ng, N. L., Murphy, S. M., Flagan, R. C., and Seinfeld, J. H.: Secondary organic aerosol formation from isoprene photooxidation, Environ. Sci. Technol., 40, 1869-1877, 2006.

Li, W., Shao, L., Buseck, P.: Haze types in Beijing and the influence of agricultural biomass burning, Atmos. Chem. Phys., 10, 8119-8130, 2010.

Li, Z., Gu, X., Wang, L., Li, D., Li, K., Dubovik, O., Schuster, G., Goloub, P., Zhang, Y., Li, L., Xie, Y., Ma, Y., and Xu, H.: Aerosol physical and chemical properties retrieved from ground-based remote sensing measurements during heavy haze days in Beijing winter, Atmos. Chem. Phys., 13, 5091-5122, 2013.

Liu, X., Li, J., Qu, Y., Han, T., Hou, L., Gu, J., Chen, C., Yang, Y., Liu, X., Yang, T., Zhang, Y., Tian, H., and Hu, M.: Formation and evolution mechanism of regional haze: a case study in the megacity Beijing, China, Atmos. Chem. Phys. Discuss., 12, 16259-16292, 2012.

Lu, Z., Streets, D. G., Zhang, Q., Wang, S., Carmichael, G. R., Cheng, Y. F., Wei, C., Chin, M., Diehl, T., and Tan, Q.: Sulfur dioxide emissions in China and sulfur trends in East Asia since 2000, Atmos. Chem. Phys., 10, 6311–6331, 2010.

Lu, Z, Zhang, Q, Streets, D.: Sulfur dioxide and primary carbonaceous aerosol emissions in China and India, 1996–2010. Atmospheric Chemistry and Physics, 11: 9839-9864, 2011.

Ma, J., Xu, X., Zhao, C., Yan, P.: A review of atmospheric chemistry research in China: Photochemical smog, haze pollution, and gas-aerosol interactions. Adv. Atmos. Sci., 29, 1006-1026, 2010.

Mathur, R., Yu, S. C., Kang, D., and Schere, K. L.: Assessment of the winter-time performance of developmental particulate matter forecasts with the Eta-CMAQ modeling system, J. Geophys. Res., 113, D02303, doi:10.1029/2007JD008580, 2008.

Nenes, A., Pandis, S., and Pilinis, C.: Continued development and testing of a new thermodynamic aerosol module for urban and regional air quality models, Atmos. Environ., 33, 1553-1560, 1999.

Pruppacher, H. and Klett, J.: Microphysics of Clouds and Precipitation. Springer, New York. p. 954, 1997.

Quan, J., Zhang, Q., He, H., Liu, J., Huang, M., and Jin, H.: Analysis of the formation of fog and haze in North China Plain (NCP), Atmos. Chem. Phys., 11, 8214-8250, 2011.

Randerson, J. T., van der Werf, G. R., Giglio, L., Collatz, G. J., and Kasibhatla, P. S.: Global Fire Emissions Database, Version 2 (GFEDv2.1), Data set available on-line (http://daac.ornl.gov/) from Oak Ridge National Laboratory Distributed Active Archive Center, Oak Ridge, Tennessee, USA, doi:10.3334/ORNLDAAC/849, 2007.

Sarwar, G., Luecken, D., Yarwood, G., Whitten, G., and Carter, W.: Impact of an updated carbon bond mechanism on predictions from the CMAQ modeling system: preliminary assessment, J. Appl. Meteorol. Clim., 47, 3-14, 2008.

Seinfeld, J. and Pandis, S.: Atmospheric Chemistry and Physics. Wiley, New York, USA, 1998.

Sun, Y., Zhuang, G., Tang, A.,Wang, Y., and An, Z.: Chemical characteristics of $PM_{2.5}$ and PM_{10} in Haze-Fog episodes in Beijing, Environ. Sci. Technol., 40, 3148-3155, 2006.

565 Tao, M., Chen, L., Su, L., and Tao, J.: Satellite observation of regional haze pollution over the North
566 China Plain, J. Geophys. Res., 117, D12203, DOI: 10.1029/2012JD017915, 2012.
567 Wang, X., Sun, M., Yang, T., and Wang, Z.: Interdecadal change in frequency of dust-haze episodes in
568 North China Plain, Clim. Environ. Res. (in Chinese), 18, 165-170, 2013.
569 Wang, Y., Zhuang, G., Sun, Y., An, Z.: The variation of characteristics and formation mechanisms of
570 aerosols in dust, haze, and clear days in Beijing, Atmos. Environ., 40, 6579-6591, 2006.
571 Wu, D., Bi, X., Deng, X., Li, F., Tan, H.: Effect of atmospheric haze on the deterioration of visibility over
572 the Pearl River Delta, Acta Geogr. Sin. (in Chinese), 21, 215-223, 2007.
573 Yu, S. C., Bhave, P. V., Dennis, R. L., and Mathur, R.: Seasonal and regional variations of primary and
574 secondary organic aerosols over the continental United States: semi-empirical estimates and model
575 evaluation, Environ. Sci. Technol., 41, 4690-4697, 2007.
576 Yu, S. C., Eder, B., Dennis, R., Chu, S. H., and Schwartz, S.: New unbiased symmetric metrics for
577 evaluation of air quality models, Atmos. Sci. Lett., 7, 26-34, 2006.
578 Yu, S. C., Mathur, R., Pleim, J., Wong, D., Gilliam, R., Alapaty, K., Zhao, C., and Liu, X.: Aerosol
579 indirect effect on the grid-scale clouds in the two-way coupled WRF-CMAQ: model description,
580 development, evaluation and regional analysis, Atmos. Chem. Phys. Discuss., 13, 25649-25739,
581 2013.
582 Yu X, Zhu B, Yin Y, Yang, J., Li, Y., and Bu, X.: A comparative analysis of aerosol properties in dust and
583 haze-fog days in a Chinese urban region. Atmos. Res., 99, 241-247, 2011.
584 Zhang, A., Qi, Q., Jiang, L., Zhou, F., and Wang, J.: Population exposure to $PM_{2.5}$ in the urban aera of
585 Beijing, PloS one, 8, e63486, 2013.
586 Zhang, J., Miao, H., Ouyang, Z., and Wang, X.: Ambient air quality trends and driving factor analysis
587 since 1980's in Beijing, Acta Sci. Circumstantiae (in Chinese), 26, 1886-1892, 2006.
588 Zhang, J., Zhu, T., Zhang, Q., Li, C., Shu, H., Ying, Y., Dai, Z., Liu, X., Liang, A., and Shen, H.: The
589 impact of circulation patterns on regional transport pathways and air quality over Beijing and its
590 surroundings, Atmos. Chem. Phys., 11, 5031-5053, 2012.
591 Zhang, M., Gao, L., Ge, C., and Y.: Simulation of nitrate aerosol concentrations over East Asia with the
592 model system RAMS-CMAQ, Tellus B, 59, 372-380, 2007.
593 Zhang, M., Xu, Y., Zhang, R., and Han, Z.: Emission and concentration distribution of black carbon
594 aerosol in East Asia during springtime, Chin. J. Geophys., 48, 55-61, 2005.
595 Zhang, M., Uno, I., Zhang, R., Han, Z.,Wang, Z., and Pu, Y.: Evaluation of the Models-3 Community
596 Multi-scale Air Quality (CMAQ) modeling system with observations obtained during the TRACE-P
597 experiment: comparison of ozone and its related species, Atmos. Environ., 40, 4874-4882, 2006.
598 Zhao, P., Zhang, X., Xu, X., and Zhao, X.: Long-term visibility trends and characteristics in the region of
599 Beijing, Tianjin, and Hebei, China, Atmos. Res., 101, 711-718, 2011.
600 Zhao, X., Zhao, P., Xu, J., Meng, W., Pu, W., Dong, F., He, D., and Shi, Q.: Analysis of a winter regional
601 haze event and its formation mechanism in the North China Plain, Atmos. Chem. Phys., 13,
602 5685-5696, 2013.
603
604
605
606

Table 1 Aerosol size distribution parameters in RAMS-CMAQ.

Mode	Aerosol components	σ^a	r^b, μm
Aitken	ASO4[c], ANO3[d], ANH4[e], BC[f], OC[g]	1.7	0.015
Accumulation	ASO4, ANO3, ANH4, BC, OC, Dust, Sea salt	2.0	0.150
Coarse dust	Dust	3.0	0.300
Coarse sea salt	Sea salt	3.5	0.300

[a] σ is geoetric standard deviation.

[b] r is mode radius.

[c] ASO4 represents sulfate aerosol.

[d] ANO3 represents nitrate aerosol.

[e] ANH4 represents ammonium aerosol.

[f] BC represents black carbon.

[g] OC represents organic carbon.

Table 2 Statistic summary of the comparisons of $PM_{2.5}$, O_3, NO_2, and visibility between simulation and observation in Beijing

		N[a]	C_{mod}[b]	C_{obs}[c]	σ_{mod}[d]	σ_{obs}[e]	R[f]
$PM_{2.5}$	Feb	665	133.05	127.5	102.41	129.7	0.76
	Jul	663	112.78	89.92	74.09	72.98	0.43
O_3	Feb	621	15.74	16.10	14.04	14.04	0.78
	Jul	630	56.59	48.75	38.44	36.21	0.74
NO_2	Feb	672	33.94	44.18	17.59	24.98	0.75
	Jul	626	25.29	24.08	17.01	11.62	0.42
Visibility	Feb	672	10.97	10.78	6.53	7.27	0.76
	Jul	744	8.06	9.64	5.74	6.48	0.65

[a]Number of samples.

[b]Total mean of observations.

[c]Total mean of simulations.

[d]Standard deviation of observations.

[e]Standard deviation of simulations.

[f]Correlation coefficient between observation and simulation.

Table 3 The number of haze days in February and July in Beijing. Also shown are the regional and temporal average surface wind speed (m s^{-1}), and visibility (km), relative humidity (%), as well as mass concentrations (μg m^{-3}) of sulfate, nitrate, ammonium, BC, OC, and $PM_{2.5}$ during the haze days in February and July, respectively, in Beijing.

variables		February	July
Number of haze days		7	13
Wind speed		3.13	3.41
Visibility		6.22	5.73
Relative humidity		55.80	74.32
Mass concentration	Sulfate	37.99	52.32
	Nitrate	54.78	48.37
	Ammonium	30.15	33.60
	BC	13.29	4.31
	OC	19.51	5.16
	$PM_{2.5}$	174.26	148.32

Table 4 Regional and monthly average extinction contribution ratios (%) of sulfate, nitrate, ammonium, BC, OC, and other aerosols (dust, sea salt, and unspecified anthropogenic mass) in February and July, respectively, in Beijing.

	Sulfate	Nitrate	Ammonium	BC	OC	Others
Feb	22.73	29.69	17.13	5.05	13.22	12.18
Jul	39.31	24.77	21.88	0.33	3.96	9.74

Table 5 Regional and monthly average mass concentration threshold of $PM_{2.5}$ ($\mu g\ m^{-3}$) under different relative humidity from the sensitivity test in Beijing.

	70%	75%	80%	85%	88%	89%	90%
Feb	82.08	78.01	72.34	64.54	58.27	55.87	53.22
Jul	83.08	78.64	72.46	64.01	57.35	54.82	52.10

Table 6 Parameters of the exponential fit for regional and monthly average $PM_{2.5}$ mass concentration threshold of haze occurrence in Beijing.

	a	*b*	*c*	R-square
Feb	96.3276	-0.4859	0.0486	0.9997
Jul	96.8810	0.7367	0.0483	0.9997

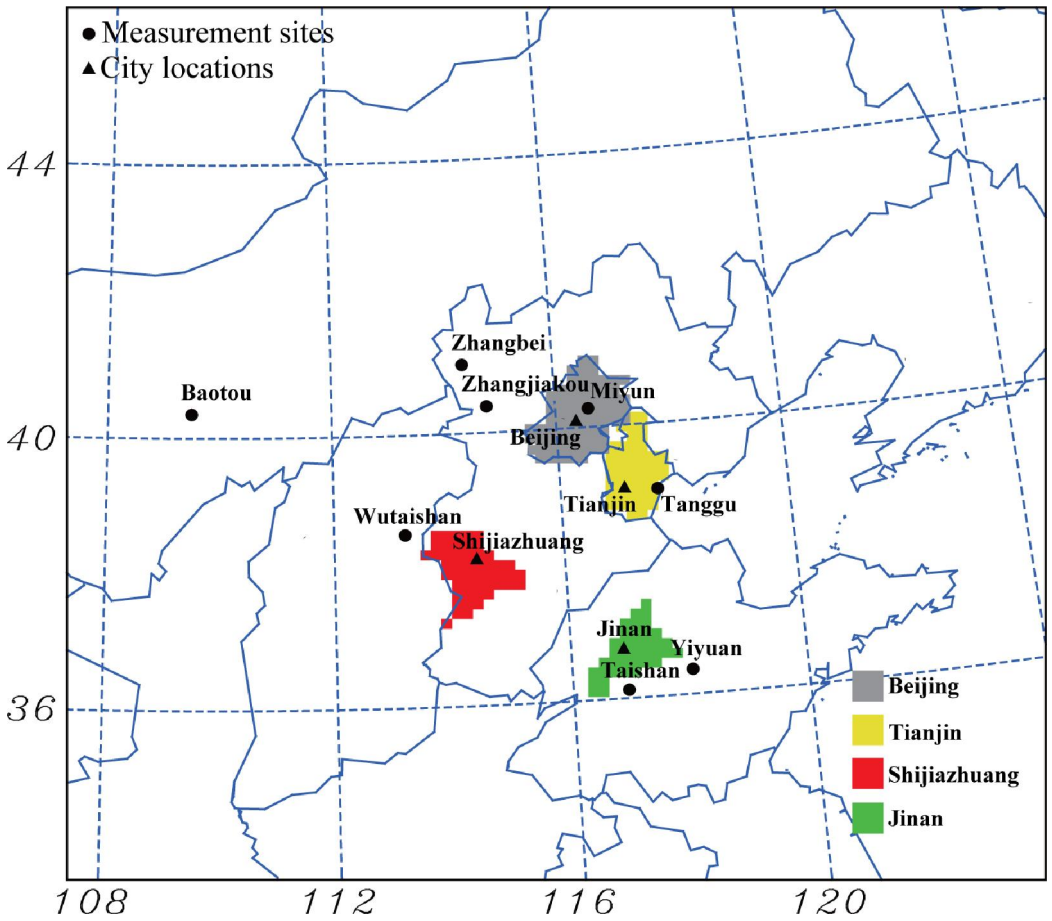

827

828 **Fig. 1.** Geographic location of API monitoring cities and CNMC measurement stations in the model domain. The gray,

829 yellow, red, and green areas represent the district of Beijing, Tianjin, Shijiazhuang, and Jinan, respectively.

830

831

832

833

834

835

836

837

838

839

840

841

842

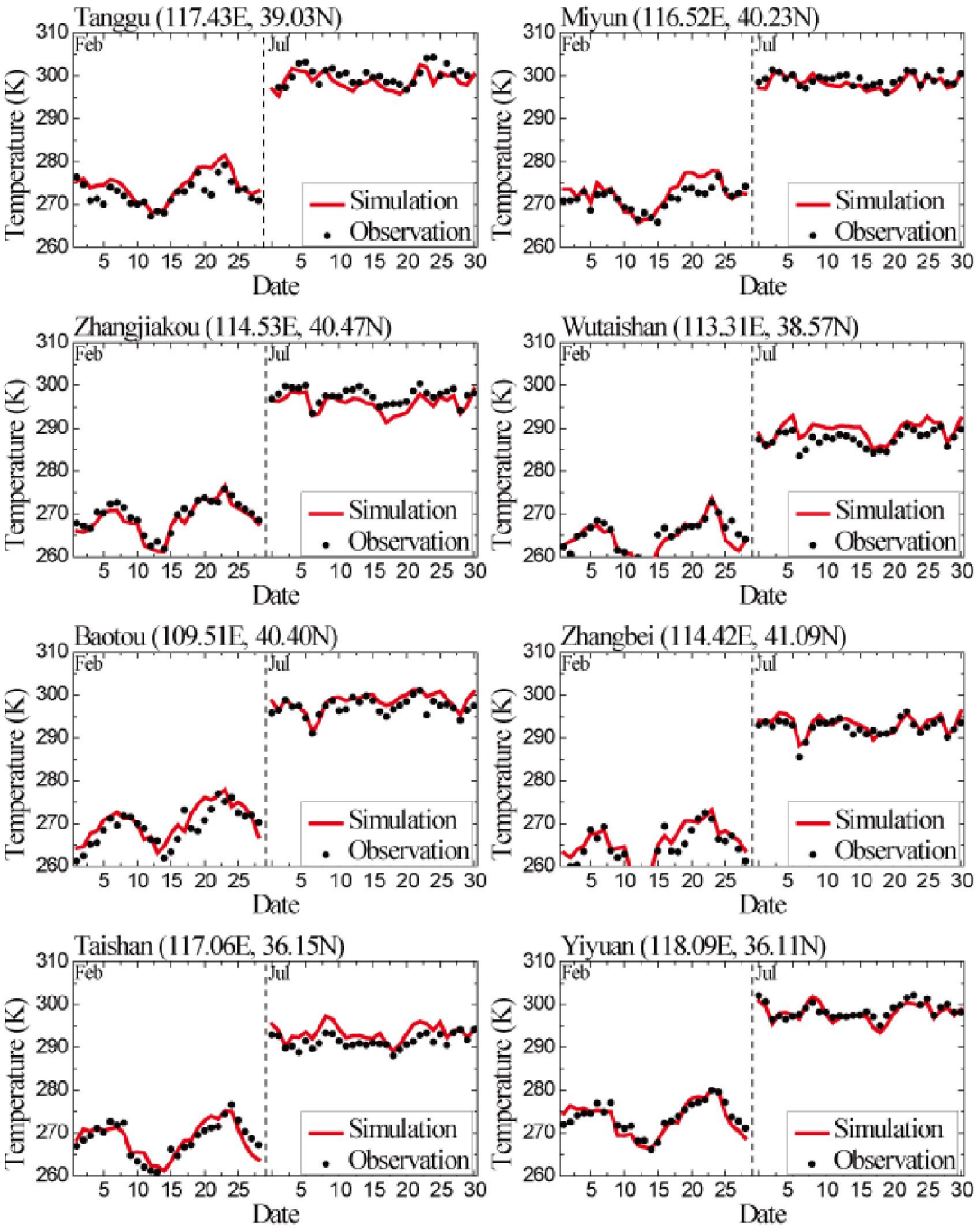

Fig. 2. Observed (circle) and modeled (solid line) daily average temperature (K) at 8 stations in February and July 2011.

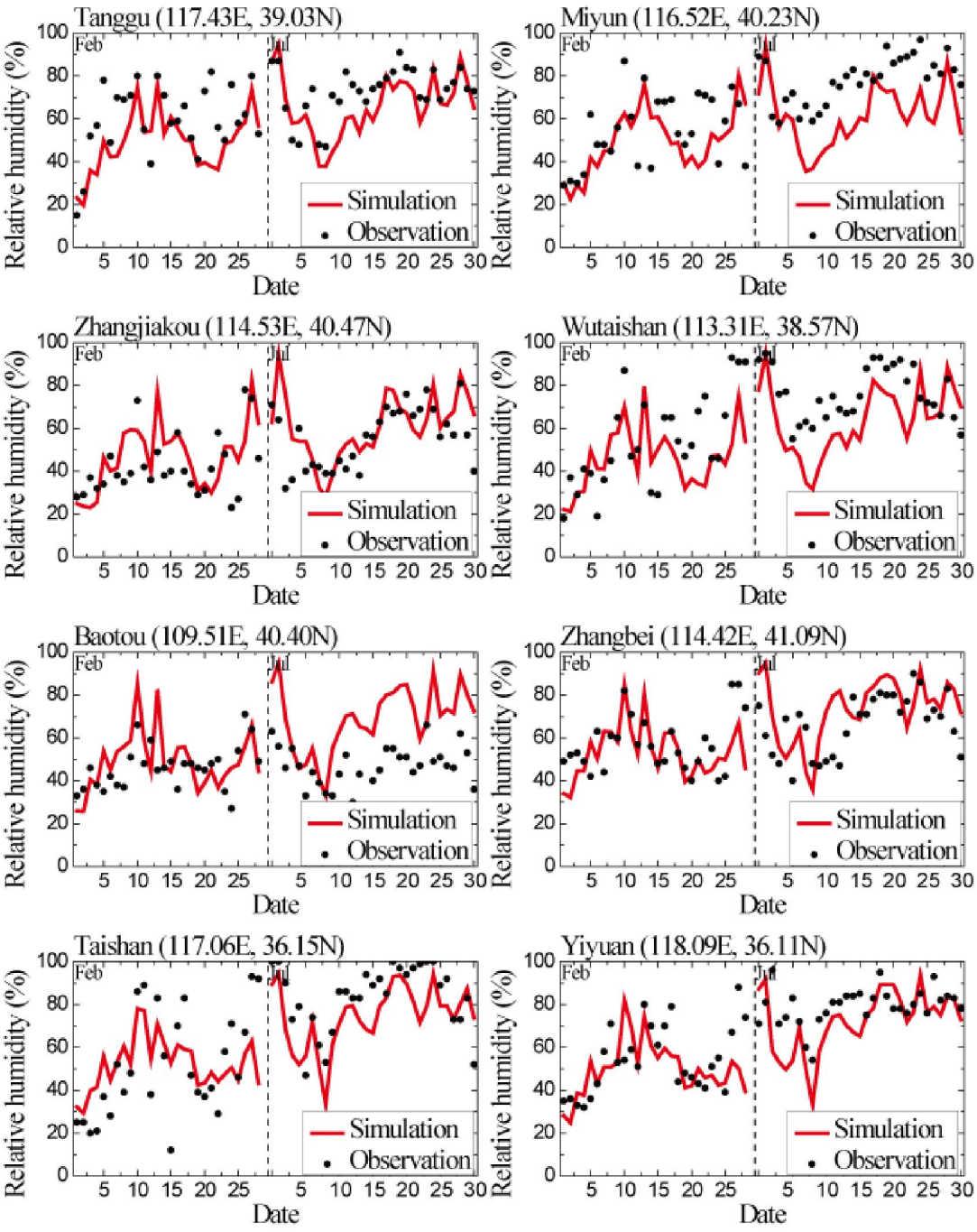

Fig. 3. Same as Fig. 2 but for relative humidity (%).

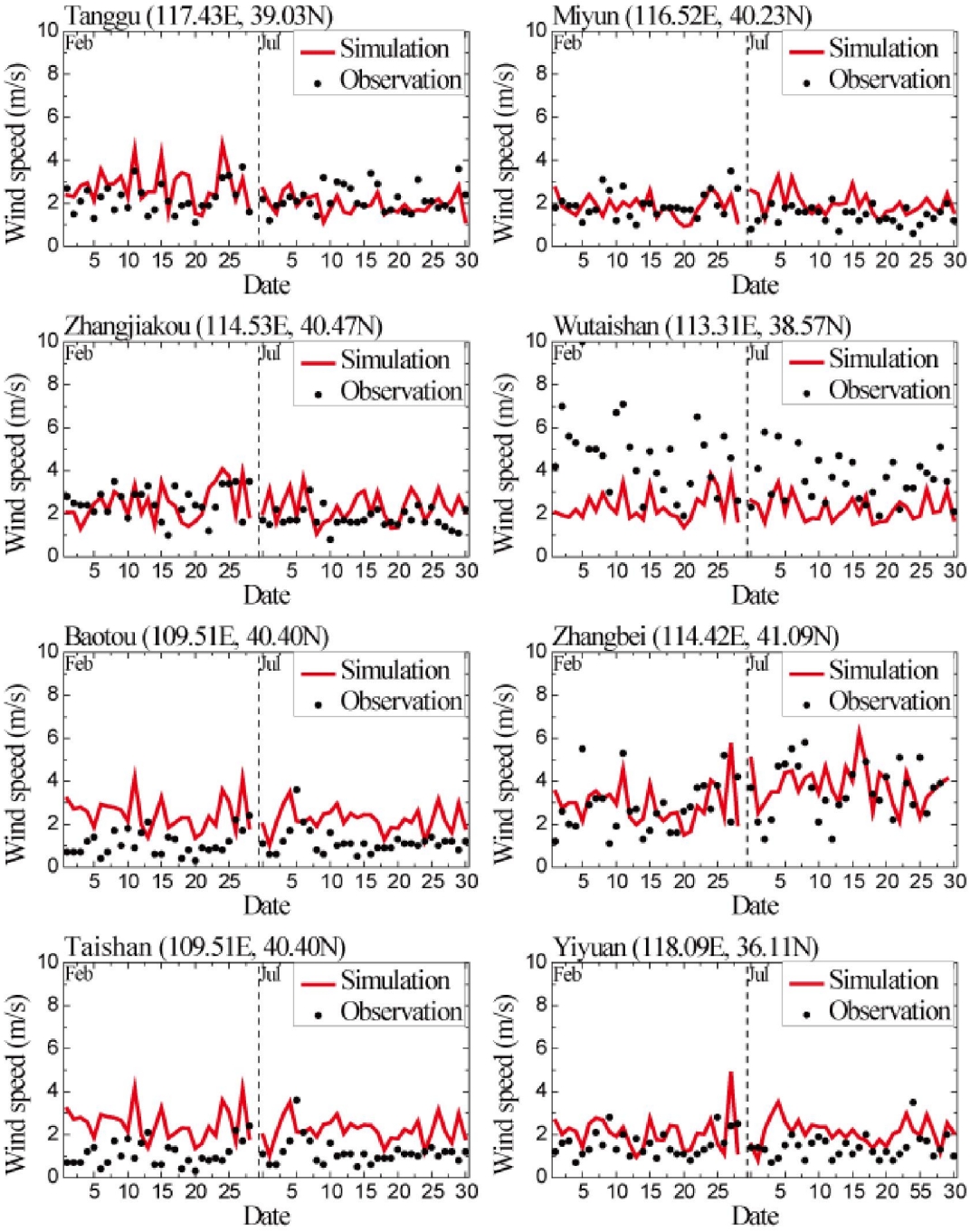

Fig. 4. Same as Fig. 2 but for wind speed (m s^{-1}).

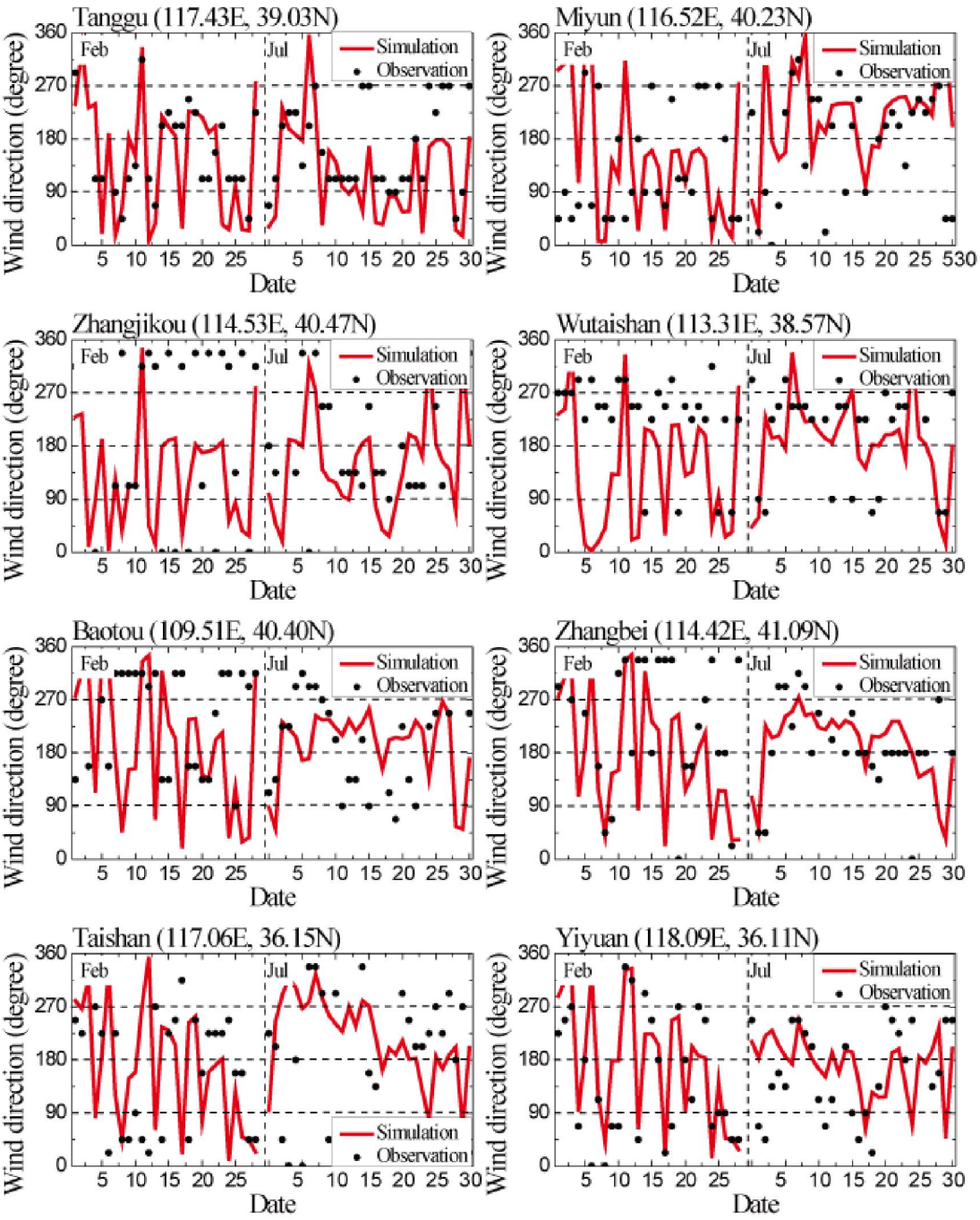

Fig. 5. Same as Fig. 2 but for wind direction (degree).

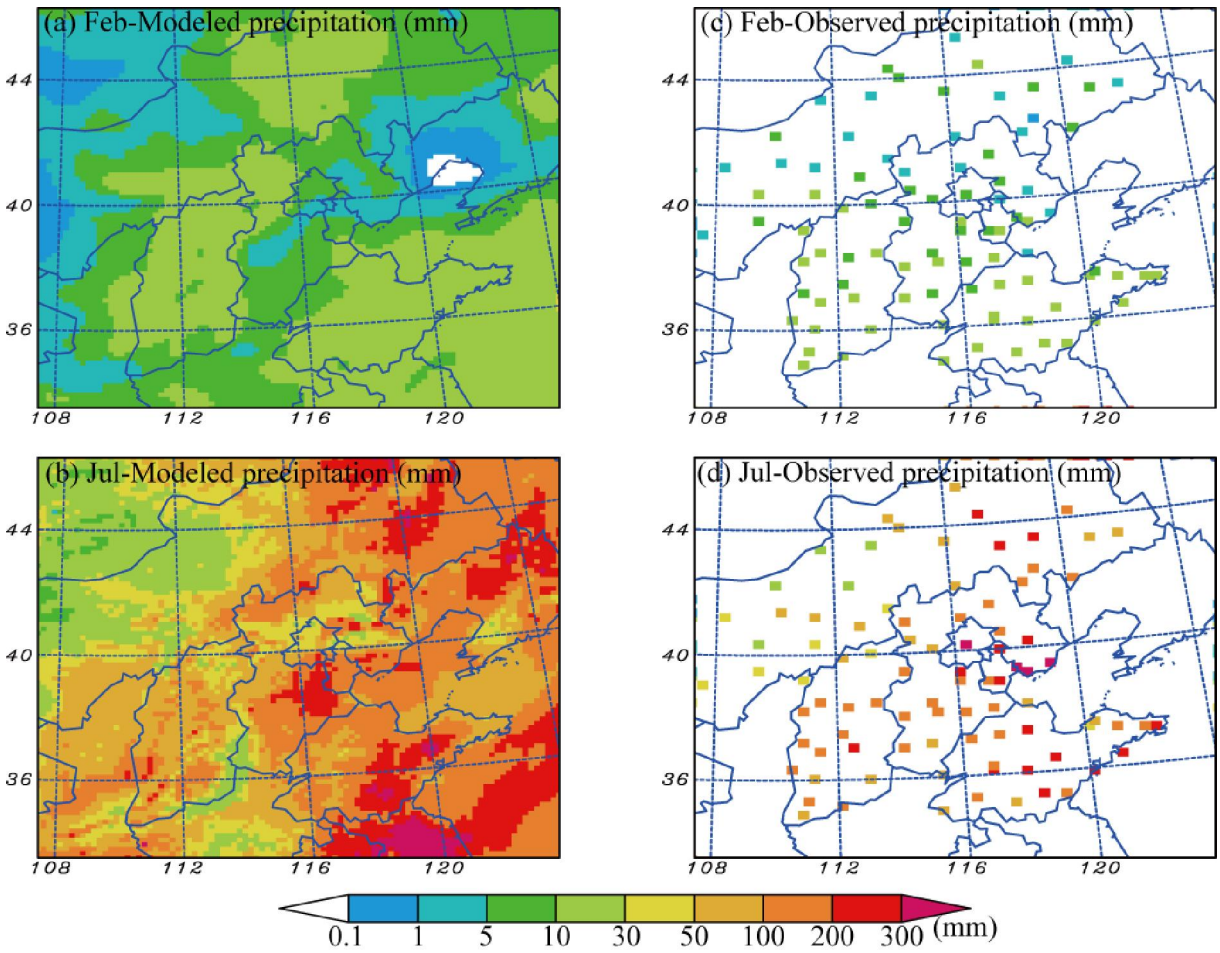

Fig. 6. The horizontal distributions of the monthly precipitation (mm) from simulation and surface observation data in February and July 2011 over NCP.

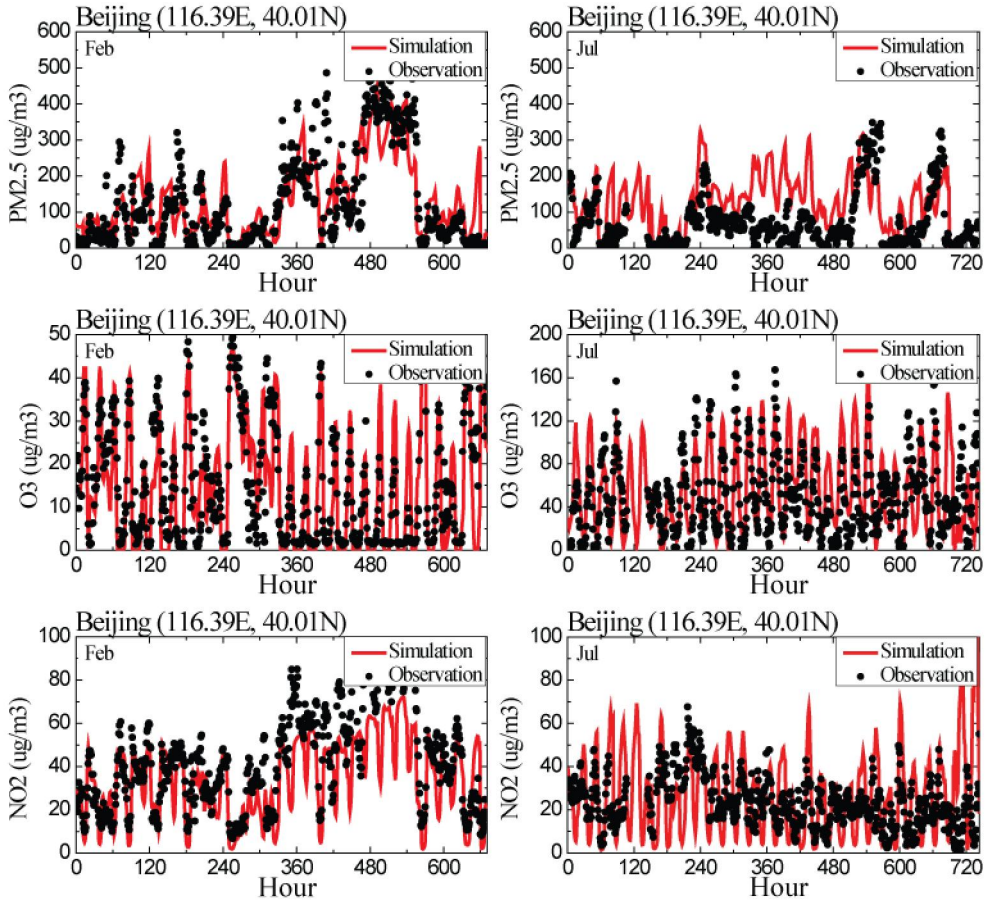

Fig. 7. Observed (circle) and modeled (line) hourly mass concentrations (μg m^{-3}) of $PM_{2.5}$, O_3, and NO_2 in February and July 2011 at Beijing.

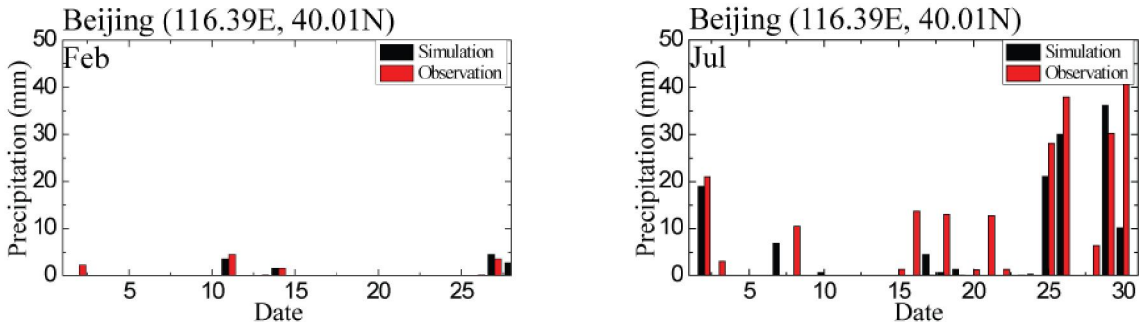

Fig. 8. Observed and modeled daily precipitation (mm) in February and July 2011 at Beijing

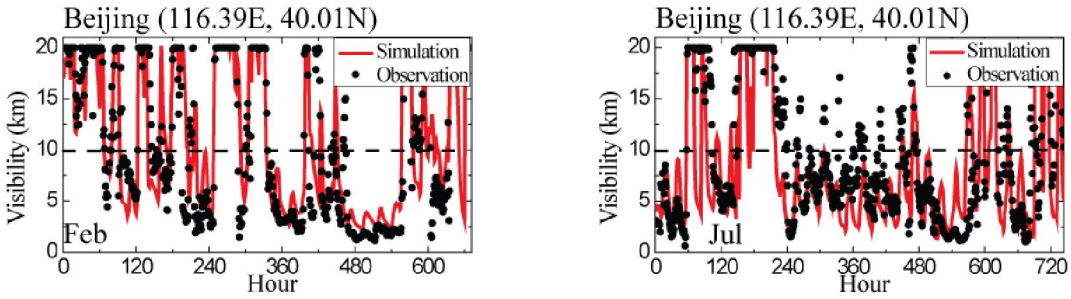

Fig. 9. Observed (circle) and modeled (line) hourly visibility (km) in February and July 2011 at Beijing.

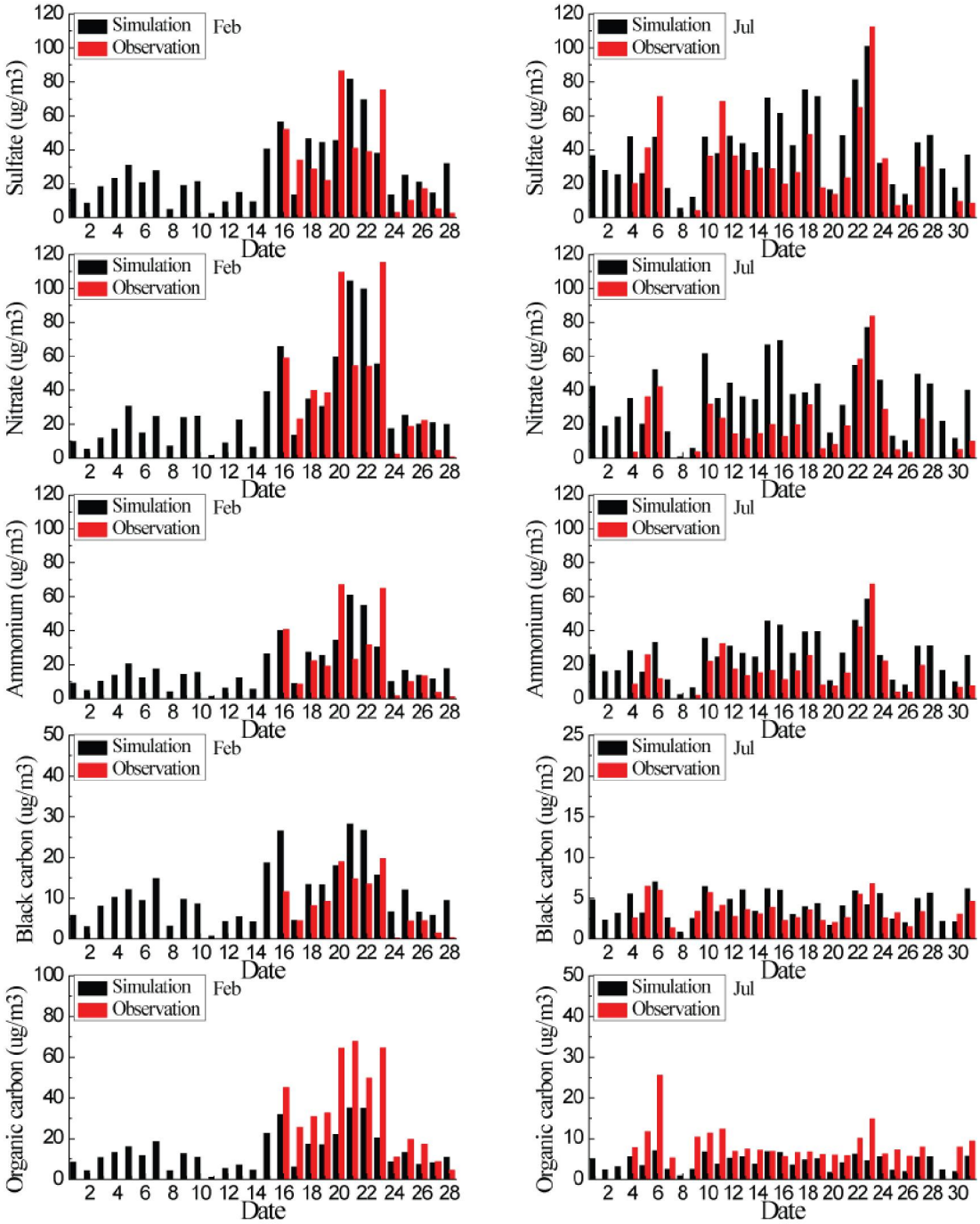

960

961 **Fig. 10.** Observed (circle) and modeled (line) daily average mass concentrations (μg m^{-3}) of sulfate, nitrate, ammonium,

962 black carbon, and organic carbon in February and July 2011 at Beijing.

963

964

965

966

967

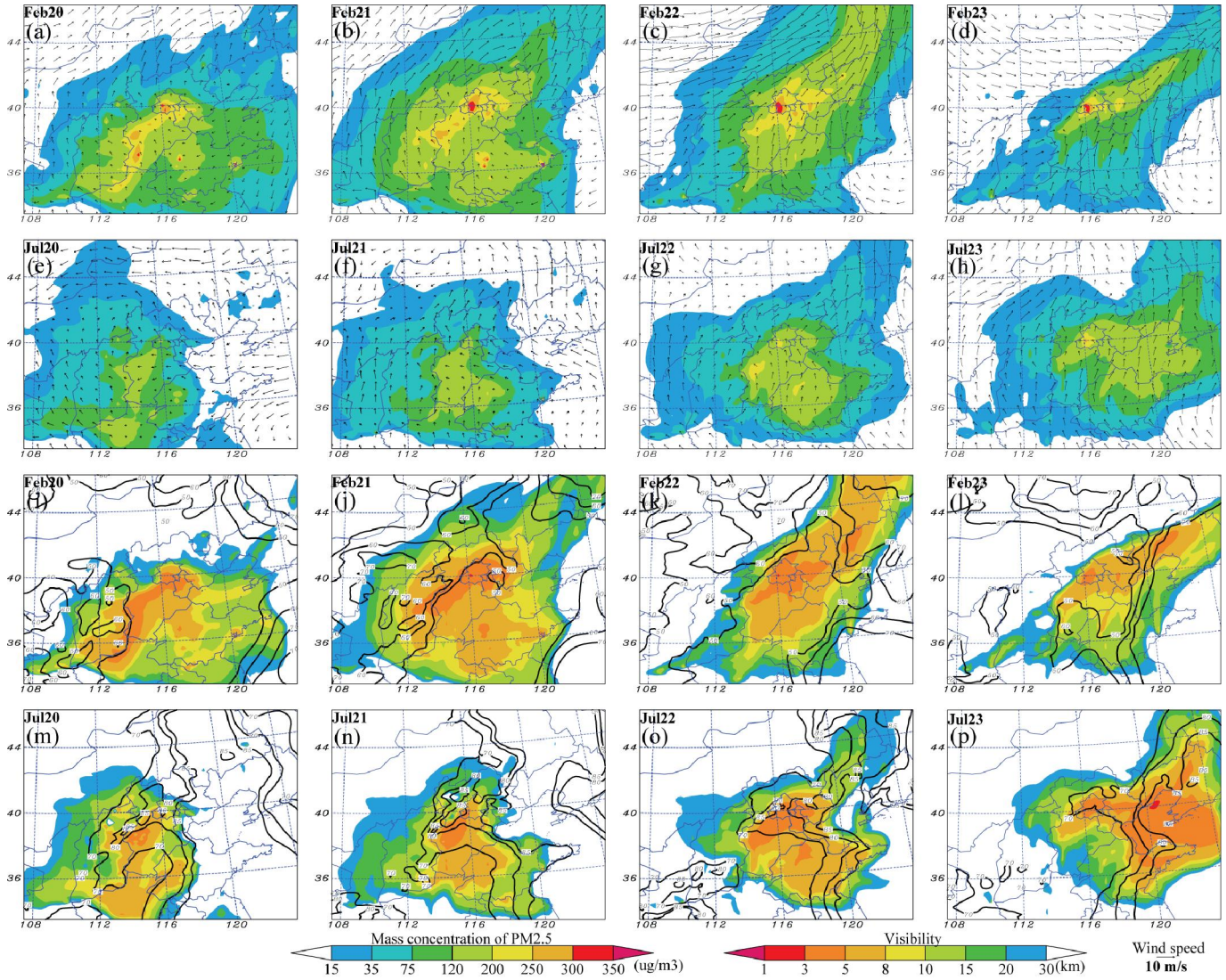

Fig. 11. The horizontal distributions of daily average mass concentration of $PM_{2.5}$ (μg m^{-3}; a-h) and visibility (km; i-p) from February 20 to 23 and July 20 to 23 over NCP. Also shown is the wind field (arrows) and relative humidity (%; black contour lines).

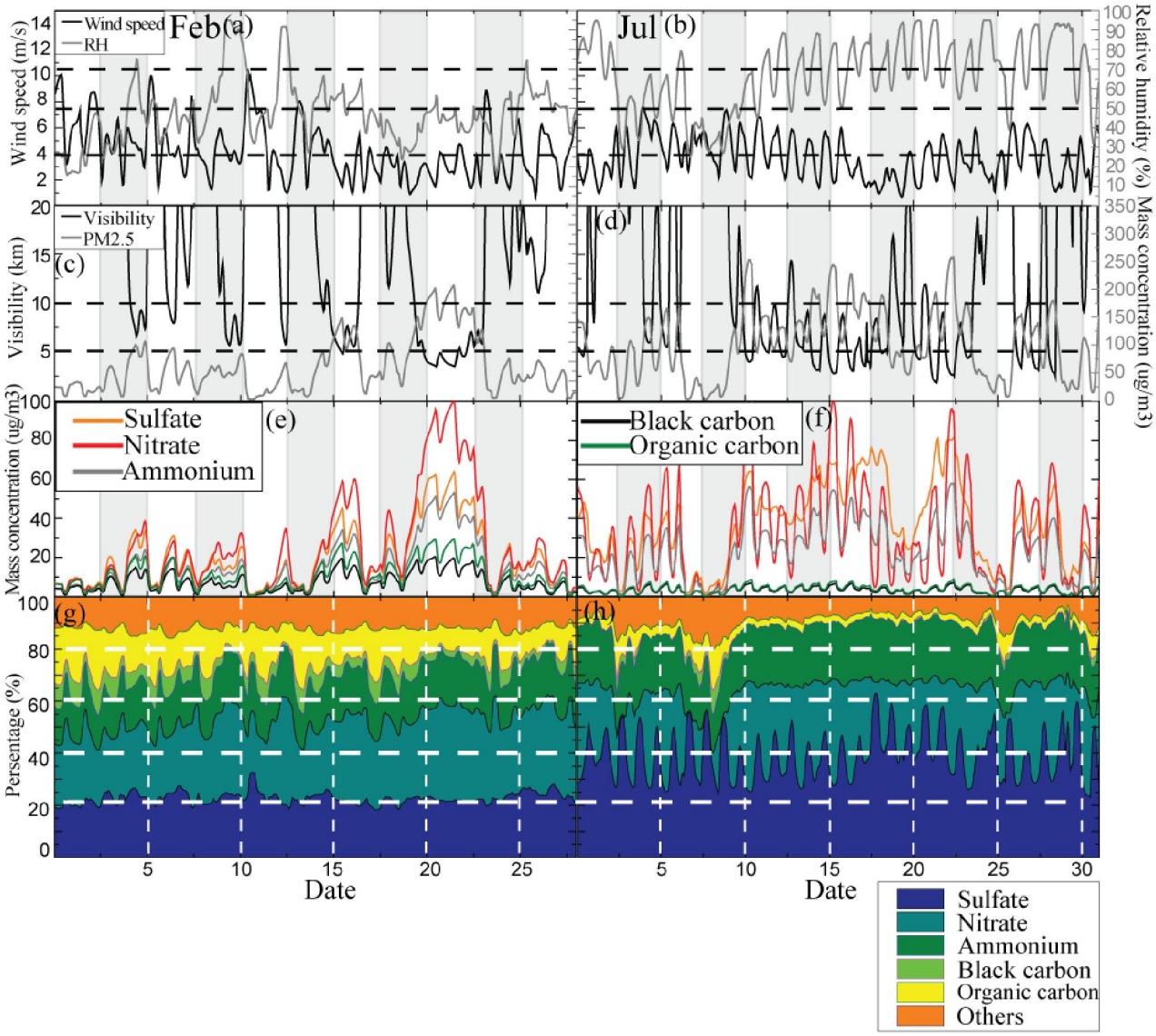

Fig. 12. The time series of regional average surface wind speed (m s^{-1}), and relative humidity (%), visibility (km), as well as $PM_{2.5}$ mass concentrations (μg m^{-3}) in February and July in Beijing (a-d). Also shown are the mass concentrations (μg m^{-3}; e-f) and extinction contribution ratios (g-h) of sulfate, nitrate, ammonium, BC, OC, and other aerosols (dust, sea salt, and unspecified anthropogenic mass).

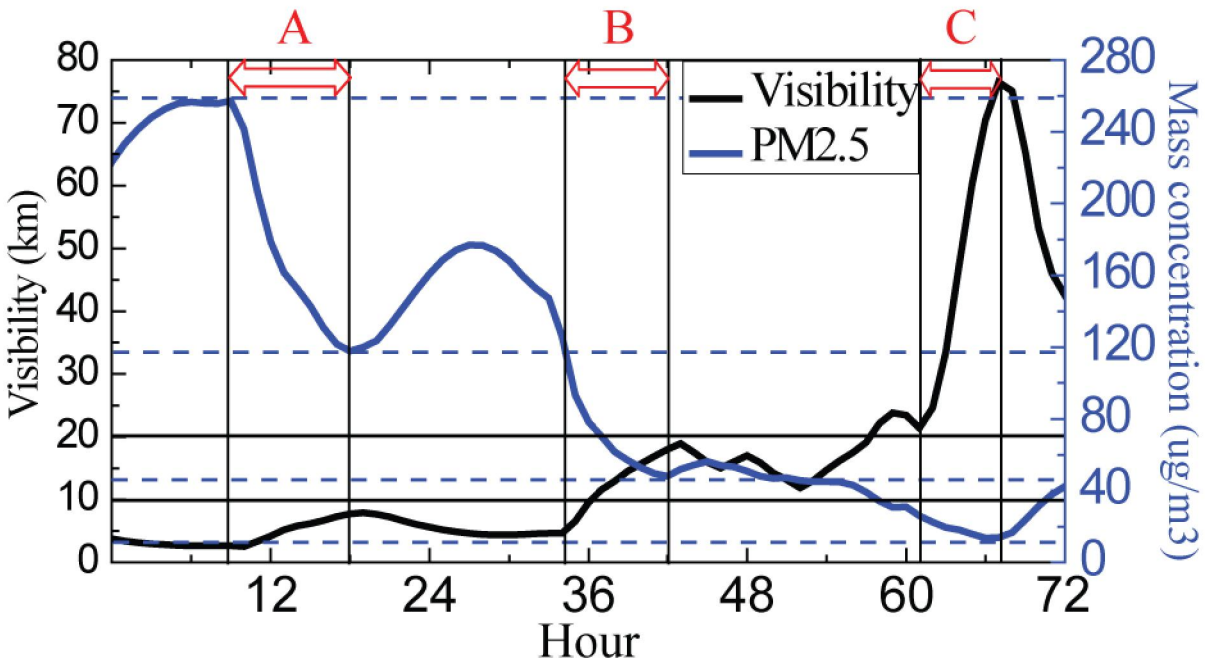

Fig. 13. The time series of regional average visibility (km) and mass concentration of $PM_{2.5}$ from July 23 to 25 in Beijing.

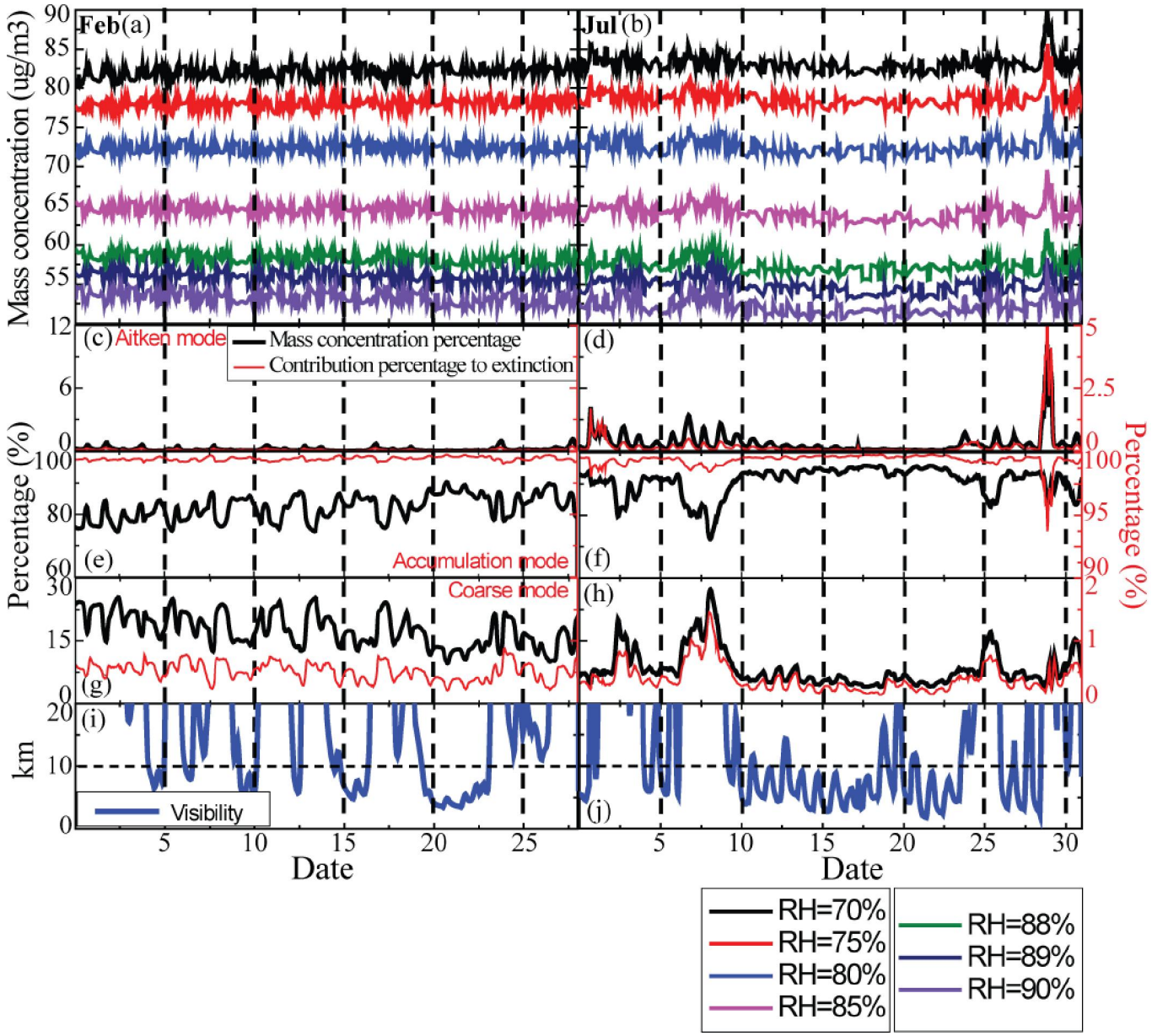

Fig. 14. The time series of regional average mass concentration threshold of $PM_{2.5}$ under different relative humidity (%) from the sensitivity test in February and July in Beijing. Also shown are the mass ratios and extinction contribution ratios (%) of Aitken mode, accumulation mode, and coarse mode, and visibility (km).

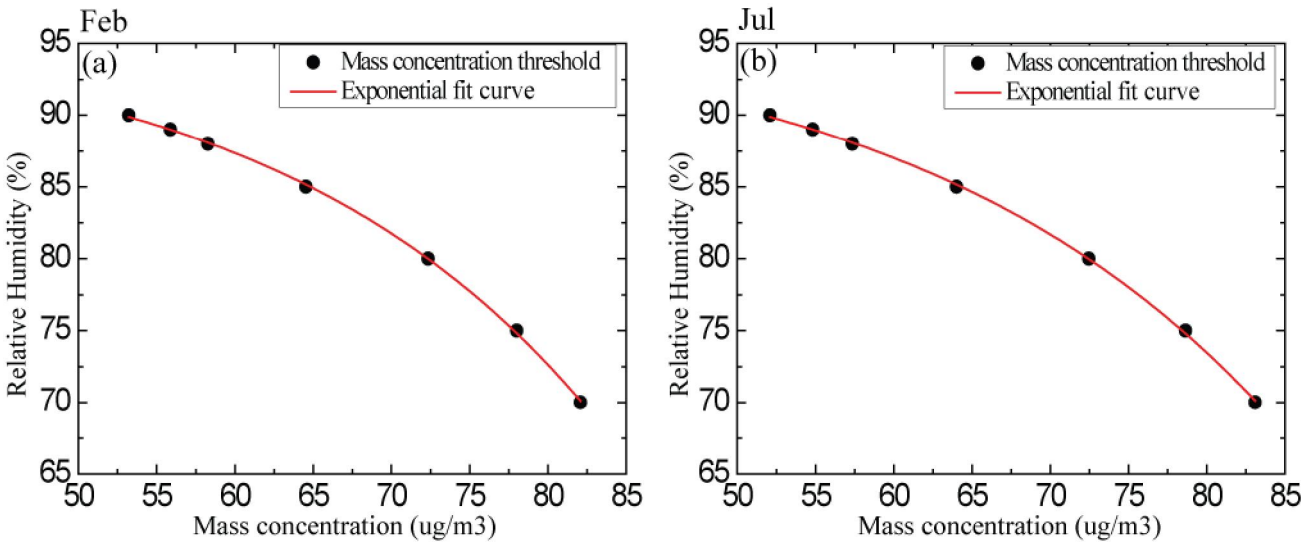

Fig. 15. The relationship between regional and monthly average $PM_{2.5}$ mass concentration threshold of haze occurrence and relative humidity in Beijing. Also shown are the exponential fit curves of the data.